ACS Catalysis

RESEARCH ARTICLE

pubs.acs.org/acscatalysis

Direct Imaging and Identification of Individual Dopant Atoms in MoS_2 and WS_2 Catalysts by Aberration Corrected Scanning Transmission Electron Microscopy

Francis Leonard Deepak,[†,‡] Rodrigo Esparza,[†] Belsay Borges,[†,§] Xochitl Lopez-Lozano,[†] and Miguel Jose-Yacaman*[,†]

[†]Department of Physics and Astronomy, University of Texas at San Antonio, One UTSA Circle, San Antonio, Texas 78249, United States

[‡]International Iberian Nanotechnology Laboratory, Avda Mestre Jose Veiga, Braga 4715, Portugal

[§]Departamento de Química, Universidad Simón Bolívar, Apartado 89000, Caracas 1080-A, Venezuela

Supporting Information

ABSTRACT: In the case of the hydrodesulfurization (HDS) processes one of the best catalysts currently available is that based on MoS_2 and WS_2. A very significant increase in their activity can be achieved by adding Co or Ni as a promoter. In the present report we have used probe aberration corrected STEM (scanning transmission electron microscopy) for the first time to characterize Co doped MoS_2/WS_2 nanowire catalysts (supported on Al_2O_3 substrates). The high-resolution imaging reveals clearly the location of Co in the individual catalysts. This has not been possible to date with other experimental techniques because of the insufficient image contrast and/or resolution. On the basis of the HAADF-STEM images, we built two models for the Co−Mo−S and Co−W−S catalysts to illustrate the different morphologies found in the catalysts. With this study it is now possible to better locate, identify, and understand the role of promoters in the design and functioning of catalysts.

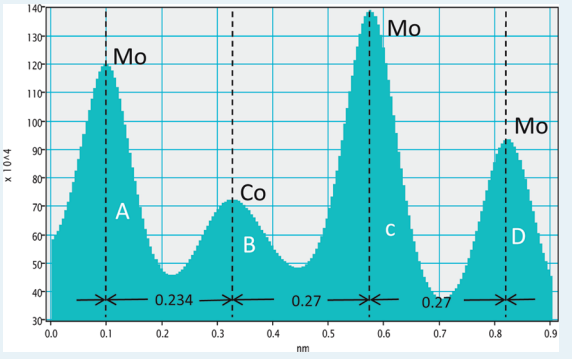

KEYWORDS: hydrodesulfurization (HDS), MoS_2 and WS_2 based catalysts, Co doped MoS_2/WS_2 nanowires, probe aberration corrected STEM

1. INTRODUCTION

Environmental regulations and new legislation demands regarding the content of sulfur in fuels have become more stringent in many countries during the past few years. Hence, there is an urgent need to improve the efficiency of catalysts used for the hydrodesulfurization (HDS) process in the oil industry.[1] One of the best catalysts currently available for HDS involves Mo or W-based catalysts, often doped with other transition metals.[2−7] While unpromoted MoS_2 (WS_2) catalysts do not possess high catalytic activity, a very significant increase in activity can be achieved by adding Co or Ni. The use of metal nanoparticles in HDS reactions has been studied with a variety of transition metals, such as Mo, Ni, Ni/Fe, Ni/W, Mo/W, and Mo/Co, which are able to hydrodesulfurize thiophene and DBT (dibenzothiophene) in good yields.[8−13] Of particular interest is the case of Co promoted MoS_2/WS_2 supported catalysts. Several investigations have been directed toward an understanding of the nature and function of the Co promoter atoms in MoS_2/WS_2 supported catalysts. Farragher[14] and Chianelli et al.[15−17] claimed that cobalt atoms at the MoS_2 edges are located between subsequent MoS_2 layers. The edge planes of MoS_2 react with Co thus becoming enriched with Co. Topsøe and Topsøe[18−22] suggested that Co atoms are located at the edge of MoS_2 platelet layers and that the edge coverage by Co atoms blocks some of the Mo adsorption sites. Bouwens et al.[23] presented a model in which the various phases can be distinguished in terms of Co−Mo coordination for two types of Co−Mo−S phases (type I: sulphidation at 673 K, type II: sulphidation at 873 K) supported on Al_2O_3, SiO_2, or carbon. They reported that in the Co−Mo−S phase the Co atoms are positioned at the edge of the MoS_2. The Al_2O_3-supported type I Co−Mo−S phase is present as a single slab structure, whereas the type II phase is present as a multilayer. SiO_2-supported Co−Mo−S phases are similar to those supported on Al_2O_3. However, the carbon-supported type II Co−Mo−S phase is similar to the type I Co−Mo−S phase supported on alumina.[24]

The difficulty for many years was to understand in detail the catalytic properties of the different types of Co−Mo−S structures since direct atom-resolved insight was not available previously. Techniques such as extended X-ray absorption fine

Received: December 14, 2010
Revised: March 25, 2011
Published: March 27, 2011

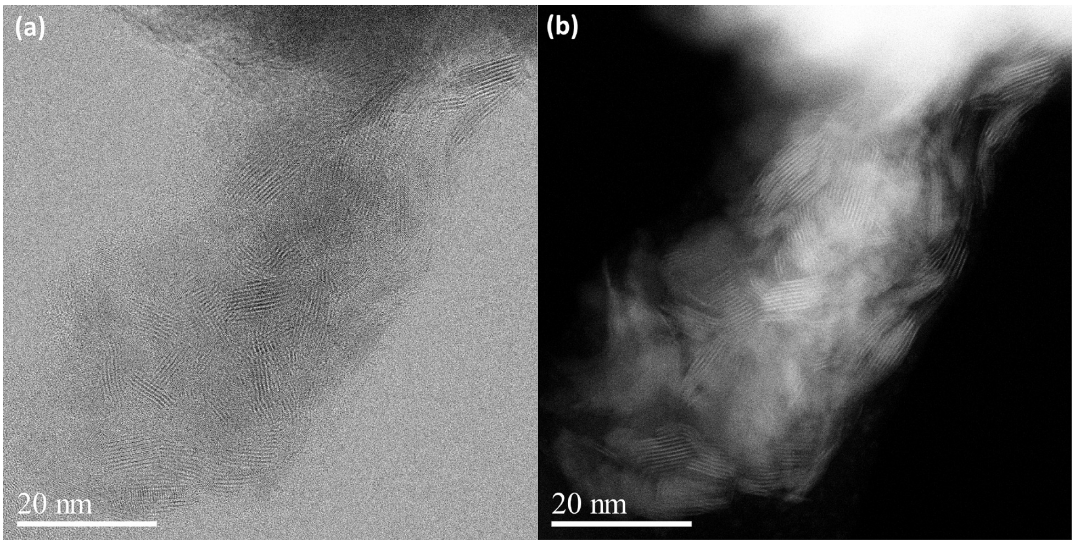

Figure 1. (a) and (b) show the low magnification BF-STEM and HAADF-STEM images of the Co-doped MoS_2 nanowire catalysts.

structure (EXAFS) and X-ray photoelectron spectroscopy (XPS) have been used to obtain information on the promoter atoms (Ex: Ni/Co) incorporated within the catalysts (Ex: MoS_2/WS_2 on Al_2O_3).[25,26] Only recently, such insight was provided by scanning tunneling microscopy (STM) along with density functional theory (DFT), and together with other advances, this has contributed greatly to improve fundamental knowledge of the MoS_2 and Co−Mo−S catalysts' structures.[27] With the advent of probe aberration corrected microscopy a solution can now be provided to the precise and direct atom-resolved understanding of these catalysts. Conventional high-resolution transmission electron microscopy (HRTEM), which has been used previously, is a powerful tool.[28−30] However, it is far less capable than high-resolution scanning transmission electron microscopy (STEM) in identifying dopant atoms. The images generated by using the high-angle scattered electrons in STEM are incoherent, giving a contrast that is strongly dependent on the atomic number Z of the observed atom. This method is therefore the most effective technique available for detecting dopant atoms incorporated within the structure of various other materials. Aberration correction has allowed sub-angstrom probes to be formed that are enormously improved in their signal-to-noise ratio and sensitivity, and are capable of visualizing single atoms with unprecedented detail.[31−33] Hence, sub-angstrom probes are crucial for imaging single atoms. In the present study we show how aberration-corrected high-angle annular dark-field (HAADF) STEM can be used to image individual cobalt atoms present in the lattice of MoS_2/WS_2 nanowire catalysts. The identification is also supported by carrying out atomic resolution energy dispersive X-ray analysis (STEM-EDAX) which can give reliable and precise chemical information to distinguish the presence of the individual promoter/dopant atoms present in the lattice of the host.[34−39] It is hoped that with such studies it may now be possible to better identify and understand the role of promoters that help enhance the activity of catalysts.

2. EXPERIMENTAL SECTION

2.1. Catalyst Preparation. *2.1.1. Preparation of the CoMo/Al_2O_3 and CoW/Al_2O_3 Supported Catalysts.* The $CoMo/Al_2O_3$ catalysts were prepared by incipient wetness impregnation of the different supports with an aqueous solution of ammonium heptamolybdate, $(NH_4)_6Mo_7O_{24}\cdot 4H_2O$. The Mo-impregnated support was then mixed with an aqueous solution of cobalt nitrate, $Co(NO_3)_2\cdot 6H_2O$ (Fluka). The catalysts were dried at 393 K and calcined under air flow at 773 K. The $CoMo/Al_2O_3$ catalyst contained 15.2 wt % MoO_3 and 4.3 wt % CoO. Sulfidation of the catalysts was carried out in a microflow reactor at 673 K—10 h at atmospheric pressure under a 10% H_2S/H_2 (v/v) sulfiding mixture. After this activation procedure, the solids were cooled to room temperature (RT) in the presence of the sulfur-containing atmosphere, flushed with an oxygen-free nitrogen flow, and stored in Schlenk tubes under argon. A similar method was employed to prepare the CoW/Al_2O_3 catalysts.[29,30]

2.1.2. Preparation of the CoMo Unsupported Catalysts. The cobalt-containing precursor, $CoCl_2\cdot 6H_2O$ was added to the red orange solution solution of $(NH_4)_2MoS_4$ in atomic proportion Co/Mo, 1:2.5. Immediately, a black precipitate is formed. The precipitate was washed several times with isopropanol before drying on a vacuum filter.

Thermal Decomposition of Co/$(NH_4)_2MoS_4$ into Co/MoS_{2+x}. The precursor was thermally decomposed under N_2 at 850 K, for 2 h (heating rate 2.5 K min^{-1}, N_2 flow: 60 cm^3 min^{-1}). At temperatures higher than 573 K, Co/MoS_{2+x} were obtained by auto reduction from MoS_3 (the value of x decreases with increasing temperature until pure MoS_2 is obtained). After this treatment, the solids were cooled down to RT under N_2 and stored in sealed bottles.[15,16,28−30] A similar procedure was employed for the synthesis of the unsupported Co/WS_2 catalyst.

2.2. Electron Microscopy Analysis. For the electron microscopy analysis, the sample was dispersed in ethanol, and a drop of this suspension was deposited onto a holey carbon grid. The samples were characterized using a JEOL, JEM-2010F (FEG-TEM) operated at 200 kV with a 0.1 nm lattice resolution, which was employed to record high resolution (HRTEM) images, obtain electron diffraction (ED) patterns, and to perform the EDX analysis of the materials. For the aberration (C_s) corrected characterization, the samples were analyzed using STEM with a JEOL ARM (200F) 200 kV FEG-STEM/TEM, equipped with a CEOS C_s corrector on the illumination system. The probe size

dx.doi.org/10.1021/cs100141p |*ACS Catal.* 2011, 1, 537–543

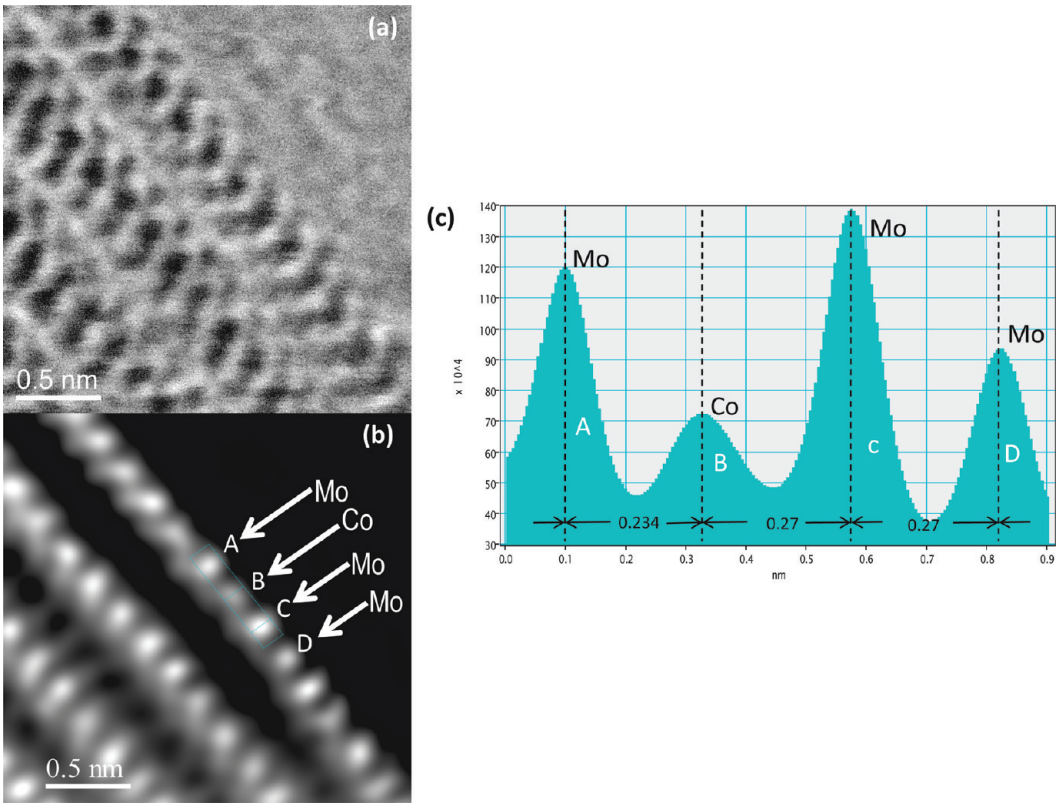

Figure 2. (a) and (b), BF-STEM and HAADF-STEM images of the Co-doped MoS_2 nanowire catalysts (unsupported catalyst), and (c) corresponding line profiles. The spacing between the Mo→Co→Mo→Mo atoms as revealed by the line profile is 2.34 Å ± 0.1 Å (Mo−Co), 2.7 Å ± 0.1 Å (Co−Mo), and 2.7 Å ± 0.1 Å (Mo−Mo) (atoms A-B-C-D). The Co atoms have a lesser intensity in comparison to the Mo atoms as a consequence of the difference in their respective atomic numbers.

used for acquiring the HAADF images as well as the BF-STEM images was the so-called condition: 9C (probe current = 32 pA, probe size used was 0.095 nm) and the condenser lens (CL) aperture size was 40 μm. High angle annular dark-field (HAADF) STEM images were acquired with a camera length of 8 cm/6 cm and the collection angle of 68−280 mrad/90−270 mrad was used. The BF-STEM images were obtained using a 3 mm/1 mm aperture and a collection angle of 17 mrad/5.6 mrad was used (camera length in this case was 8 cm). The HAADF as well as the BF images were acquired using a digiscan camera.[40] To reduce the noise of the images and to obtain clearer images the raw data was filtered using the 2D Wiener filter and the Richardson−Lucy/Maximum Entropy algorithm implemented by Ishizuka.[41] The EDAX analysis was performed using EDAX instrumentation attached to the JEOL-ARM microscope. Spectra, line scans as well as chemical maps for the various elements were obtained using the EDAX genesis software. For the EDAX analysis the probe size used was the so-called condition: 6C (probe current = 140 pA, probe size = 0.13 nm) and the CL aperture size was 40 μm.

3. RESULTS AND DISCUSSION

Figure 1a and 1b shows the low magnification BF-STEM and HAADF-STEM images of the Co-doped MoS_2 nanowire catalysts. Large amounts of the nanowires can be clearly seen in the images. A closer look at the nanowires is provided by the high resolution STEM images in Figure 2. Figure 2a and b shows the BF-STEM and HAADF-STEM images of the Co-doped MoS_2 nanowires. From the image (Figure 2b, see also Supporting Information, Figure S1) and the line profile (Figure 2c) drawn along the row of the bright atomic columns interesting variations in the atomic spacing are revealed. The spacing between the atoms varies from 2.34 Å (±0.1 Å) to 2.7 Å (±0.1 Å) (atoms A and B vs B and C) (bright atom contrast revealing the Mo−Co−Mo interatomic distances). The final Mo−Mo interatomic distance is 2.70 Å (±0.1 Å) (atoms C and D). This is indeed interesting and can be explained in terms of the substitution of Co into the lattice of Mo, occupying the Mo-sites. In addition one can also note the difference in the atom contrast (between Mo and Co, Figure 2b) which decreases on going from the Mo→Co and subsequently increases from Co→Mo (see also Supporting Information, Figure S2). The interlayer distances as measured from the line profile of the individual layers is found to be 5.84 Å. The variations on the HAADF contrast cannot be explained on the basis of thickness changes. Therefore, most important contributions should originate from compositional variations, revealed by the difference in atomic number (Z) that exists among molybdenum (atomic number = 42) and cobalt (atomic number = 27). The HAADF intensity is considered to be proportional to $Z^{1.7}$. It is well established that the projected atomic columns in HAADF-STEM images appear in bright contrast. Since the images are incoherent, no interference effects are produced between the Bloch waves propagating through the crystal and thus the contrast strongly depends on the atomic number.[42−44] Finally it should be noted that in between the layers the presence of the S atoms that make up the S−Mo−S can be inferred from their lighter contrast in comparison to the

dx.doi.org/10.1021/cs100141p |ACS Catal. 2011, 1, 537–543

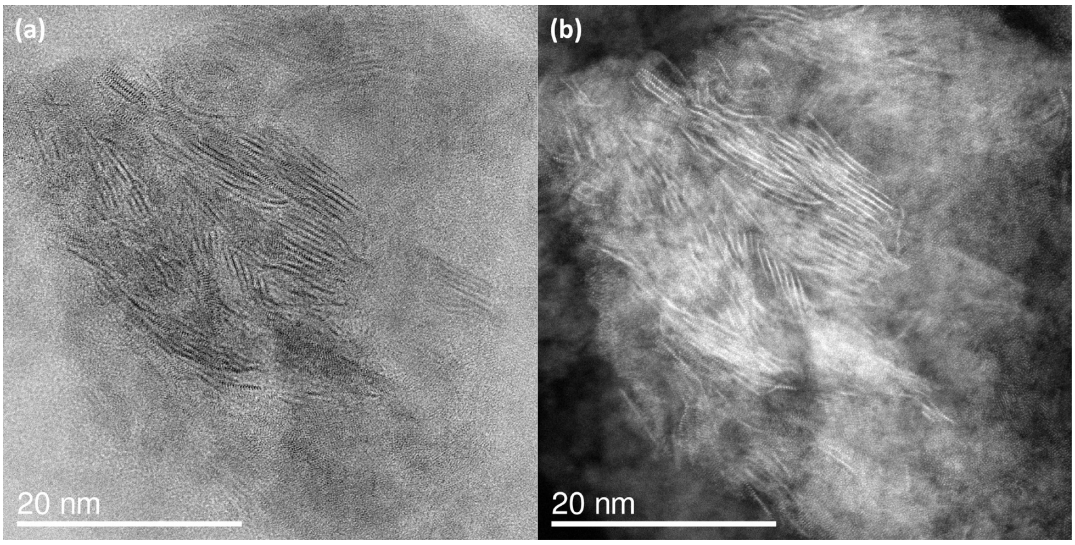

Figure 3. (a) and (b) show the low magnification BF-STEM and HAADF-STEM images of the Co-doped WS_2 nanowire catalysts supported on alumina.

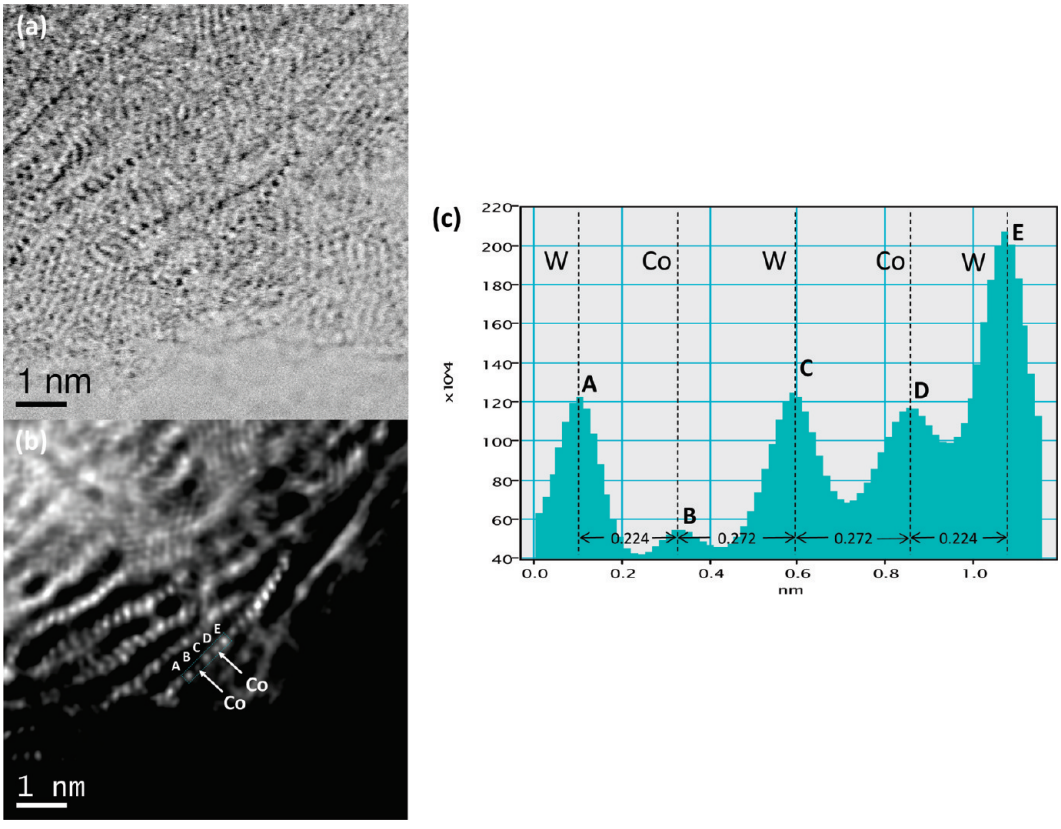

Figure 4. (a) and (b), BF-STEM and HAADF-STEM images of the Co-doped WS_2 nanowire catalysts (supported on Al_2O_3) and (c) corresponding line profiles. The spacing between the W−Co−W−Co−W atoms as revealed by the line profile is 2.24 ± 0.1 Å (W−Co), 2.72 ± 0.1 Å (Co−W), 2.72 ± 0.1 Å (W−Co), 2.24 ± 0.1 Å (Co−W), (atoms A→B→C→D→E). The Co atoms have a lesser intensity in comparison with the W atoms because of the difference in their respective atomic numbers.

brighter Mo/Co atoms. The identification of Co present uniformly throughout the MoS_2 catalysts was ascertained by carrying out EDAX spectra (see Supporting Information, Figures S3).

Figure 3a and b shows the low magnification BF-STEM and HAADF-STEM images of the Co-doped WS_2 nanowire catalysts supported on alumina substrate. Large amounts of the nanowires can be clearly seen in the images. Figure 4a and b, shows the high resolution BF-STEM and HAADF-STEM images of the Co-doped WS_2 nanowire catalyst. From the images (Figure 4b, see also Supporting Information, Figure S4) and the line

dx.doi.org/10.1021/cs100141p |*ACS Catal.* 2011, 1, 537–543

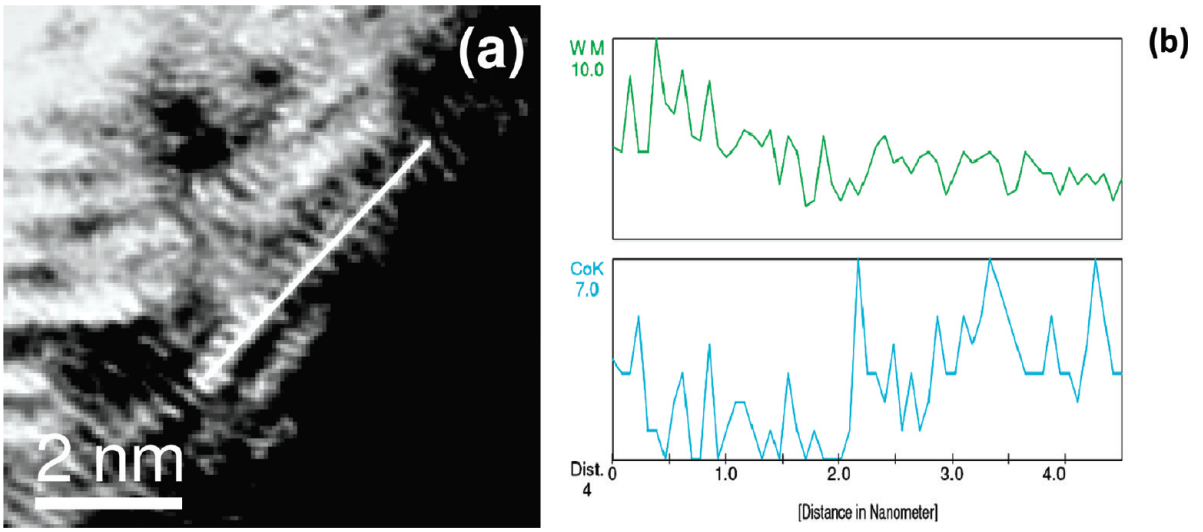

Figure 5. EDAX line scans carried out on an individual Co-doped WS_2 nanowire catalyst. The presence of the characteristic and distinct signals of W (M) and Co (K) have been identified from the line scan (Co present at the W-sites).

profile (Figure 4c) drawn along the row of the bright atomic columns, variations in the interatomic spacing is observed. The spacing between the atoms varies from 2.24 Å (±0.1 Å)−2.72 Å (±0.1 Å)−2.72 Å (±0.1 Å)−2.24 Å (±0.1 Å) (atoms A−B−C−D−E) (bright atom contrast revealing the W−Co−W−Co−W interatomic distances). This variation in the interatomic distances can be explained in terms of the substitution of Co in the lattice of W (akin to the case of Co atoms substituting Mo as explained before). In addition one can also note the difference in the atom contrast (between W and Co, Figure 4b, atoms W−Co−W−Co−W (A−B−C−D−E)). The variations are due to the difference in atomic number (Z) between tungsten (atomic number = 74) and cobalt (atomic number = 27). Also the intensity variations in the HAADF line scans is dependent on the thickness of the atomic layers themselves (whether it is 1−2−3 layers). This also the reason why it appears that the Mo/W bright atoms contrast appears elongated (two or more layers are twirled and hence produce this type of effects, see for example, Figure 4b (for the Co:WS_2 case) and Figure 2b (for the Co:MoS_2 case) where this entanglement of the WS_2/MoS_2 layers can be clearly seen).

Figure 5b shows the EDAX line scan carried out on one of the individual Co-doped WS_2 nanowires (see the image, Figure 5a). The characteristic W (M) and the Co (K) signals are obtained from the line scans indicating the presence of W and Co to be present in the individual WS_2 nanowire (Co incorporated at the W-sites). The EDAX spectra thus supports the previous HAADF-STEM observations that Co is indeed present in the lattice of WS_2 (see Figure 4). In addition the identification of Co present uniformly throughout the WS_2 catalysts was ascertained by carrying out EDAX spectra and line scans over the entire catalyst (see Supporting Information, Figures S5 and S6). Finally we have not been able to identify CoS_2 as a possible secondary phase and thus conclude that Co is indeed present only as a dopant in the MoS_2/WS_2 systems studied here.

MoS_2 is a layered material consisting of weakly bounded S−Mo−S sheets, and a single layer can be terminated by two different edges: the molybdenum- terminated edge (10−10) (Mo-edge) and the sulfur-terminated (−1010) edge (S-edge). The Mo-edge exposes a row of Mo atoms with a coordination of only four S atoms. The S-edge corresponds to an edge where the Mo atoms are fully saturated with S atoms. Density functional theory (DFT) calculations concentrate on the adsorption of sulfur on the Mo-terminated edges and the formation of vacancies on the S-terminated edges to investigate the nature of the catalytic properties of MoS_2.[45,46]

In past two decades, numerous configurations for the S-adsorption and the cobalt-promoter distribution at the Mo- and S-active-edges of MoS_2 have been intensively investigated by different theoretical and experimental groups.[45,46] One of the most relevant DFT simulation results shows that, for typical HDS conditions, the energy of the S-edge with 100% Co is lower than the Mo-edge with 100% Co.[45−50] However, in addition to the affinity of Co for the S-edge under such reaction conditions, new calculations by Krebs et al.[47,48] recently revealed that a 50% Co-promoter decoration of the Mo-edge reduces considerably the edge energy of the Mo-edge, to a value close to the S-edge value. Such new feature had important consequences on the morphologies considered so far and opened a new landscape of possibilities on the location and nature of active sites at the edges of the CoMoS phase. In particular, DFT calculations showed that the 50% Co partial occupation with the Mo-edge covered by 25% S is stable. Furthermore, the simulations also indicated the existence of two configurations with such S-saturation that are close in energy, namely, the alternate configuration −Mo−Co−Mo−Co− and the paired configuration −Mo−Mo−Co−Co.[47,48] Figure 6(a) and (b) show a perspective view of these configurations together with their respective top view of the Mo-edge. In both cases, the Mo-edge structure exhibits mixed Co−Mo sites while the S atom is located at the top of the Mo atoms. Nevertheless, it was also found that S atoms might also be located in bridging positions which indicated that the mobility of S-atoms on the Mo-edge is high.[47,48] To illustrate the experimentally observed morphologies, we built two models for the Co−Mo−S and Co−W−S catalysts [see Figure 6(c) and (d)]. Figure 6(c) shows the atomic model for the MoS_2 doped with Co for the experimentally found −Mo−Co−Mo−Mo− sequence indicated previously in Figure 2(b). In contrast with the simulations, where the optimized local Co−Mo distances are comprised between 2.74 Å and 2.84 Å, the pairing of the Mo_1 and Co_1 edge atoms (2.34 Å) is observed,

dx.doi.org/10.1021/cs100141p |*ACS Catal.* 2011, 1, 537–543

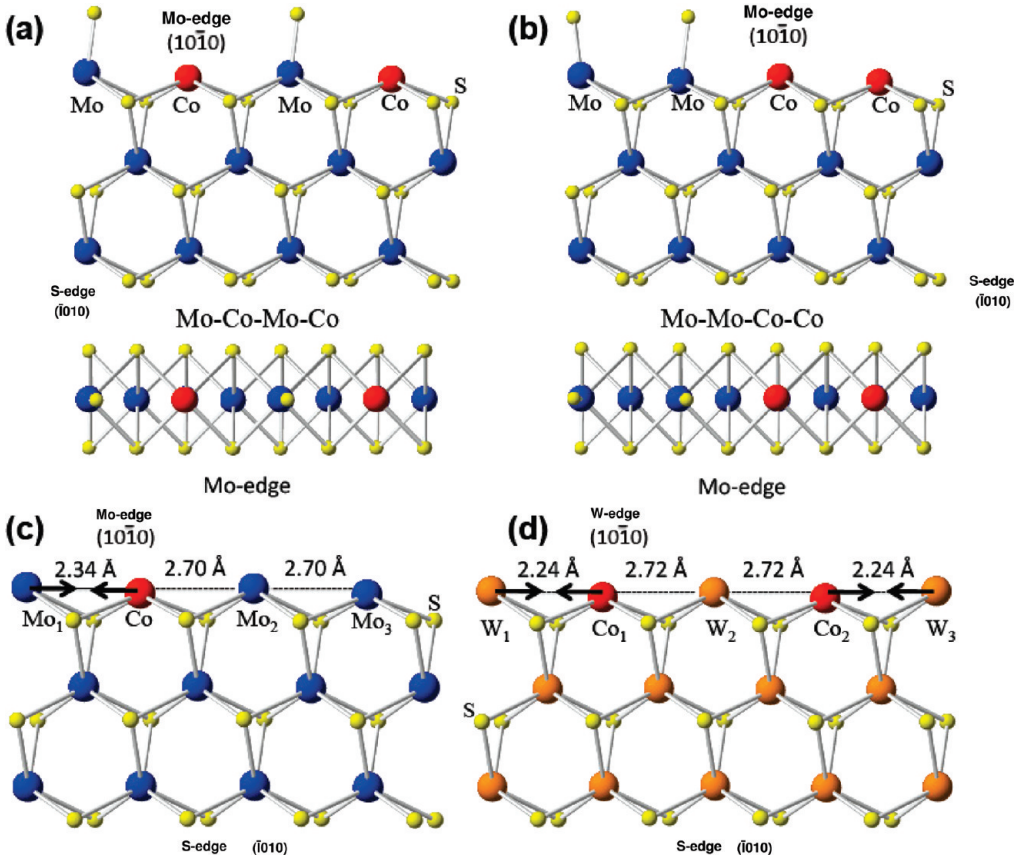

Figure 6. Perspective and top view of (a) Mo-edge with 50% Co in an alternate position and 25% S. (b) Mo-edge with 50% Co in a pairing configuration and 25% S. (c)[(d)]. Perspective view of CoMoS (CoWS) structure for the experimentally observed Mo−Co−Mo−Mo (W−Co−W−Co−W) sequence at the Mo/W-edge. Mo (W) atoms are in blue (orange) while S atoms are in yellow.

followed by a 2.70 Å separation for both Co_1-Mo_2 and Mo_2-Mo_3 atoms. Interestingly, this structure appears to be a combination of the alternate and paired configuration both very close in energy. The 100% Co−50% S and 100% Co−62.5% S configuration at the S-edge (not shown) were not experimentally observed. Figure 6(d) shows the atomic model for the Co−W−S catalysts for the sequence W−Co−W−Co−W presented in Figure 4. This model supports the idea that the Co-promoter atoms incorporate into the MoS_2 structure by substituting Mo edge atoms in an alternating configuration as it was already mentioned. Previous DFT calculations indicate that under reaction conditions, 50% S coverage on the promoted W edge and S edge are the most energetically stable configurations. In contrast with the CoMoS model, the S atoms are located at the bridging positions according to Sun et al.[51,52] Additional DFT calculations are desirable to reveal in detail the S-saturation configuration at the W-edge. In general, the exact location of the S atoms, and as a consequence the location of the active edges, remains an issue at the experimental level since it is not yet possible to distinguish between 25% or 50% of S-saturation at the Mo edge when S atoms are located on top of the Mo-edge atoms.

4. CONCLUSION

Co-doped MoS_2/WS_2 nanowire catalysts were studied by aberration corrected (C_s) STEM imaging to understand the catalytic active edges and their shape. Atomic-resolved information of the presence of the dopant (Co) was clearly established in the individual nanowires. Such direct atom imaging in the case of doped MoS_2/WS_2 catalysts has not been possible previously. The HAADF images allow to confirm the main features of two competing models nearly degenerate in energy previously suggested by DFT calculations for Co-doped MoS_2 catalyst. Both models indicated the substitution and alternation of the Co-promoter at the Mo/W-edge.

■ ASSOCIATED CONTENT

Supporting Information. Figure S1−S7, HAADF-STEM images of the Co-doped MoS_2/WS_2 catalyst, EDAX spectrum and line scans of the doped catalysts. This material is available free of charge via the Internet at http://pubs.acs.org.

■ AUTHOR INFORMATION

Corresponding Author

*E-mail: miguel.yacaman@utsa.edu. Phone: (210) 458-5451. Fax: (210) 458-4919.

■ ACKNOWLEDGMENT

The authors would like to acknowledge the NSF PREM Grant DMR 0934218 titled "Oxide and Metal Nanoparticles- the Interface between Life Sciences and Physical Sciences".

REFERENCES

(1) U.S. Environmental Protection Agency (http://www.epa.gov/otaq/gasoline.htm). European Union, EU Directive 98/70/EC, 1998.
(2) Angelici, R. J. In *Encyclopedia of Inorganic Chemistry*; King, R. B., Ed.; John Wiley & Sons: New York, 1994; p 1433.
(3) Topsøe, H.; Clausen, B. S.; Massoth, F. E. *Hydrotreating Catalysis: Science and Technology*; Springer-Verlag: Berlin, 1996.
(4) Kabe, T.; Ishihara, A.; Qian, W. *Hydrodesulfurization and Hydrodenitrogenation:Chemistry and Engineering*; Kondasa-Wiley-VCH: Tokyo, 1999.
(5) Sanchez-Delgado, R. A. *Organometallic Modeling of the Hydrodesulfurization and Hydrodenitrogenation Reactions*; Kluwer Academic Publishers: Dordrecht, 2002.
(6) Angelici, R. J. *Organometallics* **2001**, *20*, 1259–1275.
(7) Angelici, R. J. *Polyhedron* **1997**, *16*, 3073–3088.
(8) Yoosuk, B.; Kim, J. H.; Song, C.; Ngamcharussrivichai, C.; Prasassarakich, P. *Catal. Today* **2008**, *130*, 14–23.
(9) Senevirathne, K.; Burns, A. W.; Bussell, M. E.; Brock, S. L. *Adv. Funct. Mater.* **2007**, *17*, 3933–3939.
(10) Brorson, M.; Carlsson, A.; Topsøe, H. *Catal. Today* **2007**, *123*, 31–36.
(11) Escalona, E. E.; Pereira-Almao, P. R.; Castillo, J.; Hung, J.; Bolıvar, C.; Scott, C. E. *Catal. Lett.* **2006**, *112*, 227–230.
(12) Olivas, A.; Alonso, G.; Fuentes, S. *Topics Catal.* **2006**, *39*, 175–179.
(13) Dhas, N. A.; Suslick, K. S. *J. Am. Chem. Soc.* **2005**, *127*, 2368–2369.
(14) Farraghher, A. L. *Adv. Colloid Interface Sci.* **1979**, *11*, 3–41.
(15) Chianelli, R. R.; Ruppert, A. F.; Behal, S. K.; Kear, B. H.; Wold, A.; Kershaw, R. *J. Catal.* **1985**, *92*, 56–63.
(16) Berhault, G.; Araiza, L. C.; Moller, A. D.; Mehta, A.; Chianelli, R. R. *Catal. Lett.* **2002**, *78*, 81–90.
(17) Rao, C. N. R.; Pisharody, K. P. *Prog. Solid State Chem.* **1975**, *10*, 207–270.
(18) Topsøe, N. Y.; Topsøe, H. *J. Catal.* **1983**, *84*, 386–401.
(19) Lauritsen, J. V.; Vang, R. T.; Besenbacher, F. *Catal. Today* **2006**, *111*, 34–43.
(20) Lauritsen, J. V.; Kibsgaard, J.; Olesen, G. H.; Moses, P. G.; Hinnemann, B.; Helveg, S.; Nørskov, J. K.; Clausen, B. S.; Topsøe, H.; Lægsgaard, E.; Besenbacher, F. *J. Catal.* **2007**, *249*, 220–233.
(21) Brorson, M.; Carlsson, A.; Topsøe, H. *Catal. Today* **2007**, *123*, 31–36.
(22) Besenbacher, F.; Brorson, M.; Clausen, B. S.; Helveg, S.; Hinnemann, B.; Kibsgaard, J.; Lauritsen, J. V.; Moses, P. G.; Nørskov, J. K.; Topsøe, H. *Catal. Today* **2008**, *130*, 86–96.
(23) Bouwens, S. M. A. M.; van Zon, F. B. M.; van Dijk, M. P.; van der Kraan, A. M.; de Beer, V. H. J.; van Veen, J. A. R.; Koningsberger, D. C. *J. Catal.* **1994**, *146*, 375–393.
(24) Iranmahboob, J.; Hill, D. O.; Toghiani, H. *Appl. Catal., A* **2002**, *231*, 99–108.
(25) Declerck-Grimee, R. I.; Caneson, P.; Friedman, R. M.; Fripiat, J. J. *J. Phys. Chem.* **1978**, *82*, 885–888.
(26) Bouwens, S. M. A. M.; Koningsberger, D. C.; De Beer, V. H. J.; Louwers, S. P. A.; Prins, R. *Catal. Lett.* **1990**, *5*, 273–284.
(27) Topsøe, H. *Appl. Catal., A* **2007**, *322*, 3–8.
(28) Berhault, G.; Mehta, A.; Pavel, A. C.; Yang, J.; Rendon, L.; Jose-Yacaman, M.; Araiza, L. C.; Moller, A. D.; Chianelli, R. R. *J. Catal.* **2001**, *198*, 9–19.
(29) Berhault, G.; De la Rosa, M. P.; Mehta, A.; José-Yácaman, M.; Chianelli, R. R. *Appl. Catal., A* **2008**, *345*, 80–88.
(30) De la Rosa, M. P.; Texier, S.; Berhault, G.; Camacho, G.; José Yácaman, M.; Mehta, A.; Fuentes, S.; Montoya, A.; Murrieta, F.; Chianelli, R. R. *J. Catal.* **2004**, *225*, 288–299.
(31) Nellist, P. D.; Pennycook, S. J. *Science* **1996**, *274*, 413–415.
(32) Pennycook, S. J. *Ultramicroscopy* **1989**, *30*, 58–69.
(33) van Benthem, K.; Pennycook, S. J. *Appl. Phys. A: Mater. Sci. Process.* **2009**, *96*, 161–169.
(34) Ortalan, V.; Uzun, A.; Gates, B. C.; Browning, N. D. *Nat. Nanotechnol.* **2010**, *5*, 506–510.
(35) Wang, S. W.; Borisevich, A. Y.; Rashkeev, S. N.; Glazoff, M. V.; Sohlberg, K.; Pennycook, S. J.; Pantelides, S. T. *Nat. Mater.* **2004**, *3*, 143–146.
(36) Shibata, N.; Findlay, S. D.; Azuma, S.; Mizoguchi, T.; Yamamoto, T.; Ikuhara, Y. *Nat. Mater.* **2009**, *8*, 654–658.
(37) Nellist, P. D.; Chisholm, M. F.; Dellby, M.; Krivanek, O. L.; Murfitt, M. F.; Szilagyi, Z. S.; Lupini, A. R.; Borisevich, A.; Sides, W. H., Jr.; Pennycook, S. J. *Science* **2004**, *305*, 1741.
(38) Krivanek, O. L.; Chisholm, M. F.; Nicolosi, V.; Pennycook, T. J.; Corbin, G. J.; Dellby, N.; Murfitt, M. F.; Own, C. S.; Szilagyi, Z. S.; Oxley, M. P.; Pantelides, S. T.; Pennycook, S. J. *Nature* **2010**, *464*, 571–574.
(39) Muller, D. A. *Nat. Mater.* **2009**, *8*, 263–270.
(40) Deepak, F. L.; Mayoral, A.; Steveson, A. J.; Mejía-Rosales, S.; Blom, D. A.; José-Yacamán, M. *Nanoscale* **2010**, *2*, 2286–2293.
(41) HREM Research Inc., http://www.hremresearch.com
(42) Li, Z. Y.; Yuan, J.; Chen, Y.; Palmer, R. E.; Wilcoxon, J. P. *Appl. Phys. Lett.* **2005**, *87*, 243103-1–243103-3.
(43) Ferrer, D.; Torres-Castro, A.; Gao, X.; Sepulveda-Guzman, S.; Ortiz-Mendez, U.; Jose-Yacaman, M. *Nano Lett.* **2007**, *7*, 1701–1705.
(44) Ferrer, D.; Blom, D. A.; Allard, L. F.; Mejía-Rosales, S.; Perez-Tijerina, E.; Jose-Yacaman, M. *J. Mater. Chem.* **2008**, *18*, 2442–2446.
(45) Byskov, L. S.; Hammer, B.; Nørskov, J. K.; Clausen, B. S.; Topsøe, H. *Catal. Lett.* **1997**, *47*, 177–182.
(46) Raybaud, P.; Hafner, J.; Kresse, G.; Kasztelan, S.; Toulhoat, H. *J. Catal.* **2000**, *190*, 128–143.
(47) Krebs, E.; Silvi, B.; Raybaud, P. *Catal. Today* **2008**, *130*, 160–169.
(48) Krebs, E.; Daudin, A.; Raybaud, P. *Oil Gas Sci. Technol.* **2009**, *64*, 707–718.
(49) Schweiger, H.; Raybaud, P.; Toulhoat, H. *J. Catal.* **2002**, *212*, 33–38.
(50) Byskov, L. S.; Nørskov; Clausen, B. S.; Topsøe, H. *Catal. Lett.* **2000**, *64*, 95–99.
(51) Sun, M.; Nelson, A. E.; Adjaye, J. *J. Catal.* **2004**, *226*, 41–53.
(52) Sun, M.; Nelson, A. E.; Adjaye, J. *J. Catal.* **2004**, *226*, 32–40.